Journal of Zhejiang University-SCIENCE A (Applied Physics & Engineering) in press
www.jzus.zju.edu.cn; www.springer.com/journal/11582
E-mail: jzus_a@zju.edu.cn

Research Article

https://doi.org/10.1631/jzus.A2300276

Enhancement in the Hg^0 oxidation efficiency and sulfur resistance of $CuCl_2$-modified MnO_x–CeO_x nanorod catalysts

Shujie GAO[1], Yongjin HU[1], Zhichang JIANG[1], Xiaoxiang WANG[2], Dong YE[1]✉, Changxing HU[3]

[1]*College of Quality & Safety Engineering, China Jiliang University, Hangzhou 310018, China*
[2]*Key Laboratory of Biomass Chemical Engineering of Ministry of Education, Institute of Industrial Ecology and Environment, College of Chemical and Biological Engineering, Zhejiang University, Hangzhou 310027, China*
[3]*Ningbo Tech University, Ningbo 315100, China*

Abstract: In this study, a series of $CuCl_2$-modified MnO_x–CeO_x nanorods were synthesized for the oxidation of Hg^0. The addition of $CuCl_2$ resulted in an enhancement in the catalyst's Hg^0 oxidation ability, and Hg^0 oxidation efficiency reached >97% from 150 °C to 250 °C. In the MnO_x–CeO_x catalysts, Mn^{4+} played the role of the active species for Hg^0 oxidization, but in the $CuCl_2$-doped catalysts Cl^- also contributed to Hg^0 oxidation, conferring the superior performance of these samples. The introduction of SO_2 led to a decrease in the availability of Mn^{4+}, and the Hg^0 oxidation efficiency of MnO_x–CeO_x decreased from ~100% to ~78%. By contrast, $CuCl_2$-promoted samples maintained a Hg^0 oxidation efficiency of ~100% during the SO_2 deactivation cycle due to the high reactivity of Cl^-.

Key words: Hg^0 oxidation; $CuCl_2$ modification; MnO_x–CeO_x nanorods; Sulfur resistance; Oxidation activity

1 Introduction

Mercury is recognized as one of the most dangerous pollutants of the environment and human beings owing to its characteristics of neurotoxicity and bio-accumulation (Baltrus et al., 2008; Jampaiah et al., 2019b). Coal combustion has been identified as the major anthropogenic source of mercury emissions (Ye et al., 2022b). In flue gas, mercury is generally present in the forms of particle-bound mercury (Hg^p), oxidized mercury (Hg^{2+}), and elemental mercury (Hg^0) (Ye et al., 2021). The former two species can be eliminated via wet flue gas desulfurization (WFGD) and dust removal units, while the high volatility and low solubility of Hg^0 make it difficult to be removed using existing pollution control devices (Chalkidis et al., 2019). Therefore, improving the efficiency of Hg^0 elimination is an important step towards effectively reducing mercury emissions.

Among various techniques for Hg^0 abatement, the catalytic oxidation of Hg^0 to Hg^{2+} is gaining popularity owing to the high solubility of Hg^{2+}, which can be effectively removed by subsequent desulfurization systems, thereby facilitating the elimination of Hg^0 from flue gas (Wu et al., 2017). The catalyst activity is crucial to the effectiveness of removal of Hg^0 from the entire system. Some catalysts, such as CeO_2–CoO_x–TiO_2 (Li et al., 2020), CeO_2–WO_3/TiO_2 (Yang et al., 2017b), MnO_x–CeO_2/TiO_2 (Li et al., 2012), MnO_x–CeO_x/AC (Wu, et al., 2017), and $CuCl_2$–CoO_x/TiO_2–CeO_2 (Li et al., 2017) have shown promising prospects for Hg^0 elimination. The superior oxygen storage capacity of CeO_2 can optimize the physicochemical properties of other components in the catalysts through synergistic effects, which positively affect the formation of reactive oxygen species and accelerate the oxidation of Hg^0. Consequently, a satisfactory Hg^0 oxidation efficiency of >95% can be achieved within a certain temperature range.

Based on variable flue gas conditions in real coal-fired power plants (Liu et al., 2020), many of the

✉ Dong YE, Richard32@126.com
Dong YE, https://orcid.org/0000-0001-8299-224X

Received May 22, 2023; Revision accepted July 24, 2023; Crosschecked

aforementioned catalysts can actively operate in low-Hg^0-concentration working gas (tens of $\mu g/m^3$) (Table S1). However, their effectiveness in eliminating Hg^0 from high-Hg^0-content gases (hundreds of $\mu g/m^3$) is uncertain. Additionally, exposure to SO_2-containing flue gas can lead to the sulfation of active agents, resulting in the formation of inert metal sulfates that significantly interfere with the Hg^0 elimination process (Wang et al., 2014; Ma et al., 2019). Therefore, developing a catalyst that exhibits superior activity under Hg^0-rich and SO_2-containing conditions is an urgent task with practical significance.

In a previous study we discovered that MnO_x–CeO_x nanorods exhibited a Hg^0 removal efficiency of >90% in simulated flue gas with an Hg^0 concentration of 350 $\mu g/m^3$ (Ye et al., 2023a). Compared with nanocube-shaped counterparts, samples with a nanorod micro-topology exhibited enhanced Hg^0 abatement capability. $CuCl_2$ is an active agent for Hg^0 oxidation, particularly in SO_2-containing flue gas. The active chlorine species produced from Cl^- can facilitate Hg^0 oxidation reactions, which endow $CuCl_2$-containing catalysts with satisfactory activity in the presence or absence of SO_2 (Li et al., 2013; Liu et al., 2015). Given this knowledge, doping highly active $CuCl_2$ may simultaneously enhance the Hg^0 oxidation ability and SO_2 resistance of MnO_x–CeO_x catalysts. This could be significant for reducing mercury emissions but is yet to be reported in the literature.

In this study, $CuCl_2$-promoted MnO_x–CeO_x catalysts were prepared using a combination of hydrothermal and wet impregnation methods. The Hg^0 oxidation activity and SO_2-resistance of the catalysts series were investigated using virgin MnO_x–CeO_x used as a reference. The catalytic physicochemical properties were characterized using transmission electron microscopy (TEM), X-ray diffraction (XRD), N_2-adsorption-desorption, and X-ray photoelectron spectroscopy (XPS), to understand the mechanisms behind the enhancement of Hg^0 oxidation capability and SO_2 tolerance.

2 Materials and methods

2.1 Chemicals

$Ce(NO_3)_3$ $6H_2O$ (AR: ≥99.0%, 100 g), 50 wt% $Mn(NO_3)_2$ aqueous solution (AR: 49.0%–51.0%, 500 mL), NaOH (AR: ≥96.0%, 500 g), and $CuCl_2$ $2H_2O$ (AR: ≥99.0%, 100 g) were obtained from Sinopharm Chemical Reagent Co., Ltd (China).

2.2 Catalyst preparation

MnO_x–CeO_x nanorods were synthesized using the hydrothermal technique of Ye et al. (Ye, et al., 2023a). The resulting product was then dried overnight at 80 °C and calcined at 450 °C for 4 h. $CuCl_2$-modified MnO_x–CeO_x nanorods were prepared via the wet-impregnation method (Ye et al., 2020). Finally, the sample was calcined at 450 °C for 4 h in air (Fig. S1). The samples were labeled based on the $CuCl_2$ loading amount. For instance, MC denotes the virgin MnO_x–CeO_x mixed oxide, and 5C–MC refers to the MnO–CeO_x catalyst modified with 5% $CuCl_2$.

2.3 Catalyst preparation

The catalytic performance of the catalyst series was tested in a fixed bed reactor. The working gas, with a total flow rate of 600 mL/min, comprised 5% O_2, 350 $\mu g/m^3$ Hg^0, 400 ppm SO_2 (when used), and nitrogen gas (N_2). Hg^0 vapor was generated through a mercury permeation tube placed in a water bath at 50 °C. In each test, 60 mg of the catalyst was used, corresponding to a gas hourly space velocity of 600,000 ml/(g×h). Because that the Hg^0 removal unit was located between the air pre-heater and the dust removal device, the temperature of the flue gas was always <250 °C. Considering the variable operation loads in real power plants, we evaluated the catalyst Hg^0 oxidation ability within the temperature range of 150–250 °C. The inlet (A_{in}) and outlet (A_{out}) concentrations of Hg^0 were monitored using an online mercury analyzer. The Hg^0 removal efficiency (η) was determined using the following equation:

$$\eta = 100\% \times \frac{(A_{in} - A_{out})}{A_{in}}, \quad (1)$$

2.4 Characterization

The textural structure parameters of the catalyst series were investigated by N_2 adsorption characterization, using an ASAP 2460 Version 3.01 Surface Area and Porosimetry Analyzer. The crystal information of the catalyst series was determined by X-ray

diffraction (XRD) using a PANalytical B.V. spectrometer. The scan range was set as 10–90° and the step size was 0.003°. The micro-topological structures of the investigated samples were observed using an FEI Tecnai F20 transmission electron microscope (TEM). The valence state of each element was determined by X-ray photoelectron spectroscopy (XPS) using an ESCALab220i-XL electron spectrometer from VG Scientific. The C 1s line at 284.6 eV was used for the binding energy calibration.

3 Results and discussions

3.1 Transmission electron microscopy and X-ray diffraction analysis

The micro-topological structures of the serial $CuCl_2$-promoted catalysts are shown in Fig. 1. The virgin MC appeared as nanorods with an aspect ratio of 20–40. After $CuCl_2$ modification, rod-shaped products with a relatively low aspect ratio of <10 were observed, which were attributed to the grinding behavior during the catalyst preparation stage. Fig. 1(e) illustrates the crystal structures of the catalyst, showing XRD diffraction peaks identical to those of fluorite CeO_2, indicating that the introduced $CuCl_2$ existed in an amorphous state on the MnO_x–CeO_x surfaces.

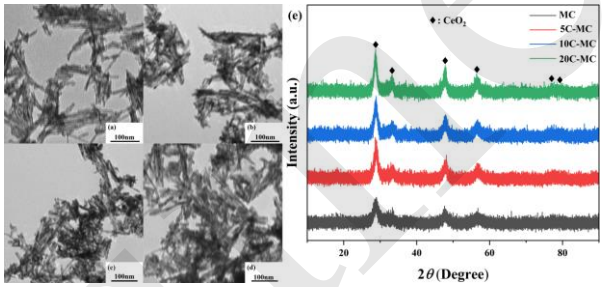

Fig. 1 TEM images: (a) MC, (b) 5C–MC, (c) 10C–MC, and (d) 20C–MC; (e) XRD patterns of the catalyst series.

3.2 N_2-adsorption-desorption analysis

The N_2-adsorption-desorption isotherms of the catalyst series are shown in Fig. S2(a). The N_2 adsorption value for all the samples showed a steep increase at a relative pressure region of P/P_0>0.8. The appearance of H3-typed hysteresis loops confirmed the presence of slit-like mesoporous structures in these catalysts (Sing and Sw, 1985). Additionally, a relatively broad pore size distribution was obtained for all the catalysts based on the results in Fig. S2(b). The specific surface area, average pore diameter, and total pore volume of the catalyst series are shown in Table 1. After 5% $CuCl_2$ was doped, the specific surface area of the catalysts decreased by ~30%. As the loading amount of $CuCl_2$ increased to 10%, the specific surface area decreased to 44 m^2/g, which was 44% lower than that of the virgin MC nanorods. Further increases in the $CuCl_2$ doping showed negligible variations in the specific surface area of the catalysts. This behavior slightly interfered with the catalyst-reactant interaction and in turn had significant impacts on the Hg^0 oxidation reactions (Ye et al., 2023a).

Phenomena such as Peierls stress, strain hardening, and fine-grain strengthening of the metallic material could appear when the load stress exceeds the proof stress. Fig. 1 is the schematic diagram of the plastic deformation of metallic materials in the precision stamping testing process.

3.3 X-ray photoelectron spectroscopy analysis

The surface atom environment of the catalyst series was investigated using the XPS technique. In the case of manganese (Mn) atoms, the curve-fitted two sub-bands at ~645 eV and ~642 eV were successively evaluated with Mn^{4+} and Mn^{3+}, respectively (Fig. S3(a)) (Ye et al., 2023b). The doping of 5% $CuCl_2$ led to a decrease in the relative content of Mn^{4+} from ~24.4% to ~22.1%. As the $CuCl_2$ loading amount increased, this value steadily decreased to 18.2% (Table 2). The change was attributed to interactions between the existing Mn species and the loaded $CuCl_2$, which subsequently altered the atom environment of Mn. Similarly, the doping of $CuCl_2$ also contributed to a decrease in the content of Ce^{4+} from 85.5% to 82.1%. The photoelectron peaks were centered at ~916, 907, 900, 898, 888, and 882 eV (Fig. S3(b)) (Jampaiah et al., 2019a). The results indicated that extraneous Cl^- interacted with Ce^{4+} species to form $CeCl_3$-like compounds, leading to an increase in the relative concentration of Ce^{3+} (Jiang et al., 2018). In the case of the copper (Cu) atoms, deconvolution of the XPS spectra revealed three sub-peaks (Fig. 2(a)). The peak with a binding energy of ~628.2 eV corresponds to Cu^+, while those in the

higher binding energy region were revealed by the presence of Cu^{2+} (Zhou et al., 2018). These findings further confirmed the interactions between $CuCl_2$ and MnO_x or CeO_x. Notably, the relative content of Cu^+ decreased from 16.9% to 7.2% as the amount of $CuCl_2$ increased, indicating that the decreased ratio of $CuCl_2$ strongly interacted with MnO_x–CeO_x binary oxide (Ji et al., 2016). Fig. 2(b) shows the Cl 2p spectra of the serial samples. The resulting two sub-bands were attributed to the spin-orbit splitting of Cl $2p_{1/2}$ and Cl $2p_{3/2}$, confirming the presence of chloride species in the form of Cl^- over the catalysts (Zhou et al., 2018).

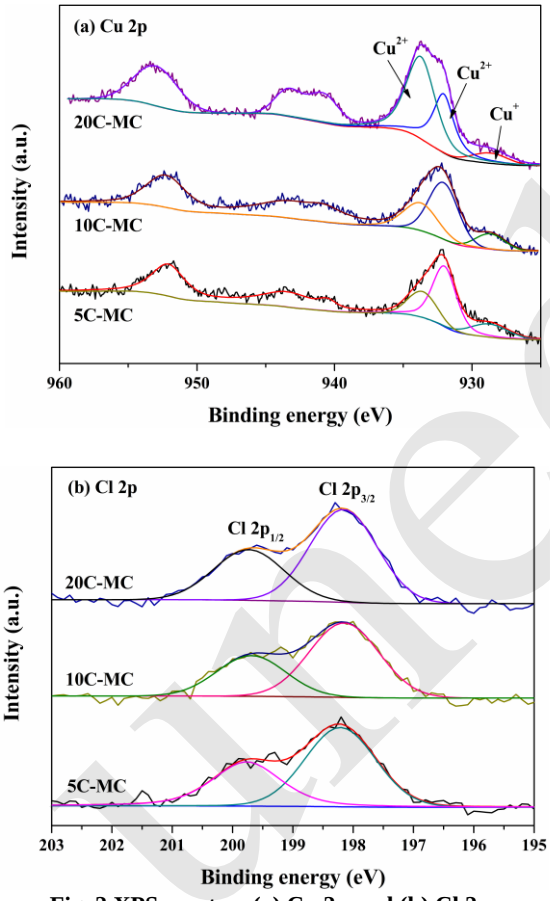

Fig. 2 XPS spectra: (a) Cu 2p and (b) Cl 2p.

3.4 Performance results

Fig. 3 shows the activity results of the examined catalysts. The virgin MnO_x–CeO_x exhibited ~100% Hg^0 removal efficiency at 150 °C. As the reaction temperature increased, the Hg^0 removal efficiency decreased, suggesting that higher temperatures significantly influenced the Hg^0 oxidation reactions. The trend was attributed to interference in the adsorption of Hg^0, leading to insufficient reactant availability for the subsequent oxidation stage and finally resulting in an inhibited high-temperature Hg^0 oxidation ability (Yang et al., 2011; Ye et al., 2022a). With the doping of $CuCl_2$, the catalyst Hg^0 removal efficiency maintained ~97% throughout the investigated temperature range, indicating an enhancement in the Hg^0 removal capability of $CuCl_2$-promoted catalysts.

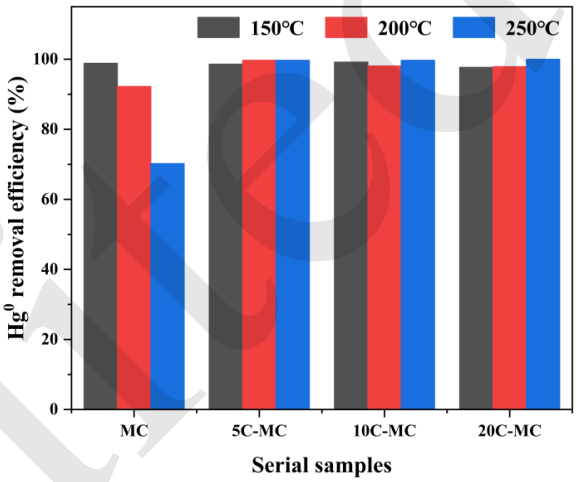

Fig. 3 Hg^0 removal efficiency of the catalyst series.

Considering that SO_2 is typically present in real coal-fired flue gas, investigating its influence on catalyst performance is essential. An Hg^0 removal efficiency of MC and 5C–MC of ~98% during the 5-h reaction cycle in the absence of SO_2 was observed, indicating the satisfactory stability of the two catalysts (Fig. 4). In this study, SO_2 was introduced into the reaction system, and the Hg^0 removal efficiency of MC steadily decreased over the reaction time. These findings confirmed that SO_2 had an inhibitory effect on the Hg^0 oxidation reactions, which was explained by the competitive adsorption of SO_2 and Hg^0 onto the catalyst active sites and the formation of inert metal sulfates (Galloway et al., 2018). In contrast, the $CuCl_2$-promoted catalyst appeared to be resistant to sulfur deactivation owing to the negligible decrease in the Hg^0 removal efficiency after 5 h of exposure to the SO_2-containing flue gas. The results indicated that the $CuCl_2$-doped MnO_x–CeO_x catalysts have satisfactory sulfur resistance.

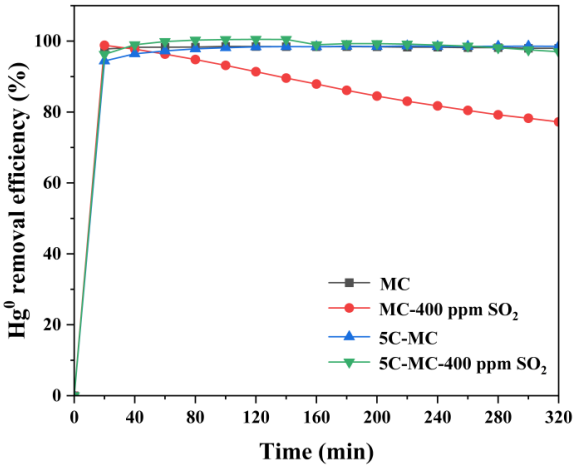

Fig. 4 SO_2-tolerance of MC and 5C–MC catalysts.

Considering the catalytic oxidation reaction of Hg^0 was similar to the increased valence state of the Hg atoms from 0 to +2, the catalyst redox properties played a significant role in this process. According to the XPS results, Mn^{4+} was the active species in the virgin MnO_x–CeO_x nanorods (Fig. S4 and Table 3). After doping with $CuCl_2$, in addition to Mn^{4+}, the Cl^- anion contributed to the oxidation of Hg^0, as shown by the decrease in the Cl content of the spent MC sample (Table 3 and Fig. S5). Under the action of oxygen and high-valence-state metal cations, Cl^- was activated into active chlorine species (Cl*), which exhibited superior reactivity and accelerated the Hg^0 oxidation process (Scheme 1) (Li et al., 2017; Yang et al., 2017a). Although the addition of $CuCl_2$ led to a decrease in the specific surface area and the content of active Mn^{4+}, this negative effect was more than offset by the promotional impact of the introduced highly active Cl^-. Consequently, the $CuCl_2$-doped catalysts had an enhanced Hg^0 oxidation ability (Ye et al., 2023a).

Furthermore, in the presence of SO_2 in the reaction systems, apart from the main reaction of Hg^0 oxidation, a side reaction involving the formation of inert metal sulfates occurred (Zhang et al., 2015; Zhang et al., 2018). Thus, the performance of the catalyst in the SO_2-containing flue gas was related to the dominance of either the main reaction or the side reaction (Zhang et al., 2018). According to the XPS results in Table 3, after the reaction in the SO_2-containing flue gas, a decrease in the content of Mn^{4+} was observed compared with the sample without SO_2 poisoning, indicating the formation of $MnSO_4$-like compounds on MnO_x–CeO_x surfaces (Zhou et al., 2022). This decrease reduced the availability of active species and subsequently inhibited the oxidation stage of Hg^0, which contributed to a decreased Hg^0 oxidation efficiency in the presence of SO_2. The $CuCl_2$-doped sample also showed a decrease in the content of Mn^{4+} after the SO_2 deactivation cycle compared with the catalyst after Hg^0 oxidation in the clean working gas, indicating the occurrence of a side reaction resulting in the formation of inert sulfate salts. Thus, Mn^{4+} contributed slightly to Hg^0 oxidation (Li et al., 2017). However, the added Cl^- compensated for this through its significant contribution to the Hg^0 oxidation reaction (Scheme 1). Subsequently, the consumption of Cl^- was accelerated, resulting in a lower amount of chlorine species remaining on the catalyst surface (Table 3). Thus, the presence of Cl^- played a significant role in obtaining the relatively high Hg^0 oxidation efficiency in the absence or presence of SO_2.

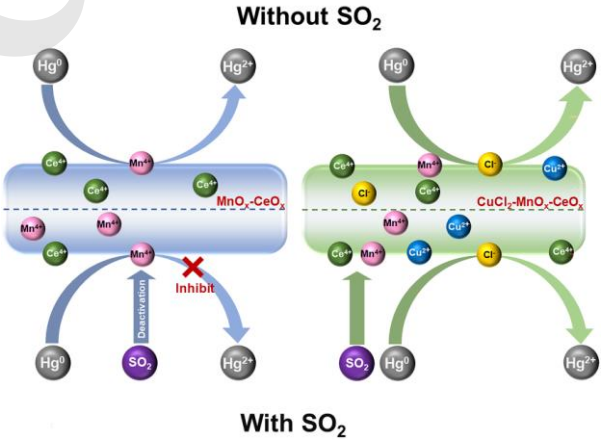

Scheme 1 Mechanisms of the enhanced Hg^0 oxidation capability and SO_2-tolerance of $CuCl_2$-doped MnO_x–CeO_x catalysts.

Table 1 Specific surface area, average pore diameter, and total pore volume of the catalyst series.

Samples	Specific surface area (m^2/g)	Average pore diameter (nm)	Pore volume (cm^3/g)
MC	78	17.2	0.50
5C–MC	53	22.6	0.44

10C–MC	44	21.0	0.35
20C–MC	43	20.8	0.31

Table 2 XPS data of the catalyst series.

Samples	Mn^{4+} (%)	Ce^{3+} (%)	Cu^{+} (%)
MC	24.4	14.5	/
5C–MC	22.1	16.0	16.9
10C–MC	20.9	17.4	14.1
20C–MC	18.2	17.9	7.2

Table 3 Measured data of the experiments in five states

Samples	Mn^{4+} (%)	Ce^{3+} (%)	Cu^{2+} (%)	Cl/(Mn+Ce+Cu)
MC	24.4	14.5	/	/
Spent MC (no SO_2)	20.0	15.0	/	/
Spent MC (with SO_2)	13.9	22.3	/	/
5C–MC	22.1	16.0	16.9	0.14
Spent 5C–MC (no SO_2)	18.2	16.1	16.6	0.11
Spent 5C–MC (with SO_2)	17.0	18.7	16.4	0.04

From an economic perspective, the improved Hg^0 oxidation efficiency resulting from the addition of $CuCl_2$ indicates that a reduced amount of catalyst was needed to meet the Hg^0 emission standards. Furthermore, the enhanced SO_2-tolerant ability indicates that the catalysts' lifespan was prolonged, reducing the need for replacements and lowering operational costs. These advantages provide guidelines for the effective reduction of mercury emissions from flue gas with high Hg^0 content (hundreds of $\mu g/m^3$) and a significant amount of SO_2 (hundreds of ppm). This method is also beneficial for achieving the goal of effectively reducing mercury emissions from industrial sources.

4 Conclusions

In this study we successfully modified MnO_x–CeO_x nanorods with $CuCl_2$ to simultaneously improve the Hg^0 oxidation capability and SO_2-tolerance of the catalysts. The following conclusions were drawn:

1. The addition of $CuCl_2$ enhances the catalyst's Hg^0 oxidation capability, with Hg^0 oxidation efficiency at >97% throughout the investigated temperature range for $CuCl_2$-doped samples. In the presence of 400 ppm SO_2, the Hg^0 oxidation efficiency of MnO_x–CeO_x steadily decreased from ~100% to ~78% after 320 min, whereas the $CuCl_2$-doped catalysts maintained ~100% Hg^0 oxidation efficiency during the SO_2 deactivation cycle.

2. For the MnO_x–CeO_x catalyst, Mn^{4+} served as the active species for Hg^0 oxidization. However, with the addition of $CuCl_2$, the introduced Cl^- with high reactivity was mainly responsible for accelerating the oxidation of Hg^0, resulting in enhanced Hg^0 oxidation capability of the $CuCl_2$-doped catalysts.

3. In the presence of SO_2, the decreased availability of Mn^{4+} largely explained the decreased Hg^0 oxidation efficiency of the MnO_x–CeO_x catalyst. However, with the addition of $CuCl_2$, Cl^- ensured the effective oxidation of Hg^0, thereby maintaining a high Hg^0 oxidation efficiency during the SO_2 deactivation cycle.

Acknowledgments

This work is supported by the Zhejiang Provincial Natural Science Foundation of China (No. LQ22E060003) and the Public Welfare Science and Technology Project of Ningbo (No. 202002N3105).

Author contributions (refer to https://www.casrai.org/credit.html)

Shujie GAO designed the research. Yongjin HU and Zhichang JIANG processed the corresponding data. Dong YE wrote the first draft of the manuscript. Xiaoxiang WANG helped to organize the manuscript. Changxing HU revised and edited the final version.

Conflict of interest

Shujie GAO, Yongjin HU, Zhichang JIANG, Xiaoxiang WANG, Dong YE and Changxing HU declare that they have no conflict of interest.

References

Baltrus JP, Granite EJ, Stanko DC, et al., 2008. Surface characterization of Pd/Al_2O_3 sorbents for mercury capture from fuel gas. *Main Group Chemistry*, 7(3):217-225. https://doi.org/10.1080/10241220802509432

Chalkidis A, Jampaiah D, Hartley PG, et al., 2019. Regenerable α-MnO_2 nanotubes for elemental mercury removal from natural gas. *Fuel Processing Technology*, 193:317-327. https://doi.org/10.1016/j.fuproc.2019.05.034

Galloway B, Royko M, Sasmaz E, et al., 2018. Mercury oxidation over Cu-SSZ-13 catalysts under flue gas conditions. *Chemical Engineering Journal*, 336:253-262. https://doi.org/10.1016/j.cej.2017.11.163

Jampaiah D, Chalkidis A, Sabri YM, et al., 2019a. Role of ceria in the design of composite materials for elemental mercury removal. *The Chemical Record*, 19(7):1407-1419. https://doi.org/10.1002/tcr.201800161

Jampaiah D, Chalkidis A, Sabri YM, et al., 2019b. Low-temperature elemental mercury removal over TiO_2 nanorods-supported MnO_x-FeO_x-CrO_x. *Catalysis Today*, 324:174-182. https://doi.org/10.1016/j.cattod.2018.11.049

Ji P, Gao X, Du X, et al., 2016. Relationship between the molecular structure of V_2O_5/TiO_2 catalysts and the reactivity of SO_2 oxidation. *Catalysis Science & Technology*, 6(4):1187-1194. https://doi.org/10.1039/c5cy00867k

Jiang Y, Lu M, Liu S, et al., 2018. Deactivation by HCl of CeO_2-MoO_3/TiO_2 catalyst for selective catalytic reduction of NO with NH_3. *RSC Advances*, 8(32):17677-17684. https://doi.org/10.1039/c8ra00280k

Li H, Wu C-Y, Li Y, et al., 2012. Superior activity of MnO_x-CeO_2/TiO_2 catalyst for catalytic oxidation of elemental mercury at low flue gas temperatures. *Applied Catalysis B: Environmental*, 111-112:381-388. https://doi.org/10.1016/j.apcatb.2011.10.021

Li H, Wang S, Wang X, et al., 2017. Activity of $CuCl_2$-modified cobalt catalyst supported on Ti-Ce composite for simultaneous catalytic oxidation of Hg^0 and NO in a simulated pre-sco process. *Chemical Engineering Journal*, 316:1103-1113. https://doi.org/10.1016/j.cej.2017.02.052

Li H, Zhang J, Cao Y, et al., 2020. Enhanced activity and SO_2 resistance of co-modified CeO_2-TiO_2 catalyst prepared by facile co-precipitation for elemental mercury removal in flue gas. *Applied Organometallic Chemistry*, 34(4) https://doi.org/10.1002/aoc.5463

Li X, Liu Z, Kim J, et al., 2013. Heterogeneous catalytic reaction of elemental mercury vapor over cupric chloride for mercury emissions control. *Applied Catalysis B-Environmental*, 132:401-407. https://doi.org/10.1016/j.apcatb.2012.11.031

Liu H, Chang L, Liu W, et al., 2020. Advances in mercury removal from coal-fired flue gas by mineral adsorbents. *Chemical Engineering Journal*, 379 https://doi.org/10.1016/j.cej.2019.122263

Liu Z, Li X, Lee J-Y, et al., 2015. Oxidation of elemental mercury vapor over gamma-Al_2O_3 supported $CuCl_2$ catalyst for mercury emissions control. *Chemical Engineering Journal*, 275:1-7. https://doi.org/10.1016/j.cej.2015.04.022

Ma Y, Mu B, Zhang X, et al., 2019. Graphene enhanced Mn-Ce binary metal oxides for catalytic oxidation and adsorption of elemental mercury from coal-fired flue gas. *Chemical Engineering Journal*, 358:1499-1506. https://doi.org/10.1016/j.cej.2018.10.150

Sing, Sw K, 1985. Reporting physisorption data for gas/solid systems with special reference to the determination of surface area and porosity. *Pure & Applied Chemistry*, 57(4):603-620. https://doi.org/10.1351/pac198557040603

Wang PY, Su S, Xiang J, et al., 2014. Catalytic oxidation of Hg^0 by MnO_x-CeO_2/gamma-Al_2O_3 catalyst at low temperatures. *Chemosphere*, 101:49-54. https://doi.org/10.1016/j.chemosphere.2013.11.034

Wu J, Zhao Z, Huang T, et al., 2017. Removal of elemental mercury by Ce-Mn co-modified activated carbon catalyst. *Catalysis Communications*, 93:62-66. https://doi.org/10.1016/j.catcom.2017.01.016

Yang S, Guo Y, Yan N, et al., 2011. Elemental mercury capture from flue gas by magnetic Mn-Fe spinel: Effect of chemical heterogeneity. *Industrial & Engineering Chemistry Research*, 50(16):9650-9656. https://doi.org/10.1021/ie2009873

Yang Y, Liu J, Zhang B, et al., 2017a. Density functional theory study on the heterogeneous reaction between Hg^0 and HCl over spinel-type $MnFe_2O_4$. *Chemical Engineering Journal*, 308:897-903. https://doi.org/10.1016/j.cej.2016.09.128

Yang Y, Liu J, Zhang B, et al., 2017b. Experimental and theoretical studies of mercury oxidation over CeO_2-WO_3/TiO_2 catalysts in coal-fired flue gas. *Chemical Engineering Journal*, 317:758-765. https://doi.org/10.1016/j.cej.2017.02.060

Ye D, Wang X, Liu H, et al., 2020. Insights into the effects of sulfate species on CuO/TiO_2 catalysts for NH_3-SCR reactions. *Molecular Catalysis*, 496:111191. https://doi.org/10.1016/j.mcat.2020.111191

Ye D, Wang X, Wang R, et al., 2021. Recent advances in MnO_2-based adsorbents for mercury removal from coal-fired flue gas. *Journal of Environmental Chemical Engineering*, 9(5):105993. https://doi.org/10.1016/j.jece.2021.105993

Ye D, Wang R, Wang X, et al., 2022a. Improvement in the Hg^0 removal performance of CeO_2 by modifying with CuO. *Applied Surface Science*, 579:152200. https://doi.org/10.1016/j.apsusc.2021.152200

Ye D, Wang X-X, Wang R-X, et al., 2022b. Review of

elemental mercury (Hg^0) removal by CuO-based materials. *Journal of Zhejiang University-SCIENCE A (Applied Physics & Engineering)*, 23(7):505-526. https://doi.org/10.1631/jzus.A2100627

Ye D, Gao S, Wang Y, et al., 2023a. New insights into the morphological effects of MnO_x-CeO_x binary mixed oxides on Hg^0 capture. *Applied Surface Science*, 613:156035. https://doi.org/10.1016/j.apsusc.2022.156035

Ye D, Hu Y, Jiang Z, et al., 2023b. Mechanistic investigation on Hg^0 capture over MnO_x adsorbents: Effects of the synthesis methods. *Journal of Zhejiang University-SCIENCE A (Applied Physics & Engineering)*, 24(1):80-90. https://doi.org/10.1631/jzus.A2200388

Zhang A, Zhang Z, Lu H, et al., 2015. Effect of promotion with Ru addition on the activity and SO_2 resistance of MnO_x-TiO_2 adsorbent for Hg^0 removal. *Industrial & Engineering Chemistry Research*, 54(11):2930-2939. https://doi.org/10.1021/acs.iecr.5b00211

Zhang D, Hou LA, Chen G, et al., 2018. Cr doping MnO_x adsorbent significantly improving Hg^0 removal and SO_2 resistance from coal-fired flue gas and the mechanism investigation. *Industrial & Engineering Chemistry Research*, 57(50):17245-17258. https://doi.org/10.1021/acs.iecr.8b04857

Zhou Z, Liu X, Hu Y, et al., 2018. An efficient sorbent based on $CuCl_2$ loaded CeO_2-ZrO_2 for elemental mercury removal from chlorine-free flue gas. *Fuel*, 216:356-363. https://doi.org/10.1016/j.fuel.2017.11.134

Zhou Z, Liu L, Liu X, et al., 2022. Catalytic oxidation of Hg^0 over Mn-doped CeO_2-ZrO_2 solid solution and MnO_x/CeO_2-ZrO_2 supported catalysts: Characterization, catalytic activity and SO_2 resistance. *Fuel*, 310:122317. https://doi.org/10.1016/j.fuel.2021.122317

Electronic supplementary materials

Table S1
Fig. S1
Fig. S2

中文概要

题　目：$CuCl_2$改性对 MnO_x-CeO_x 纳米棒催化剂汞氧化性能及抗硫性能的提升机理研究

作　者：高淑洁[1]，胡永金[1]，蒋志昌[1]，王晓祥[1]，叶栋[1]，胡长兴[3]

机　构：[1]中国计量大学，质量与安全工程学院，中国杭州，310018；[2]浙江大学，工业生态与环境研究所，化工学院，中国杭州，310018；[3]浙江大学宁波理工学院，中国宁波，315100

目　的：针对实际燃煤电站多变的烟气条件，开发适用于高汞、含硫烟气条件的催化剂是目前的研究重点。

创新点：1. 通过水热法合成锰铈氧化物纳米棒，可实现高汞烟气条件下的汞高效脱除；2. 通过 $CuCl_2$ 的添加，在保证催化剂汞氧化性能的同时还提升其抗硫性能。

方　法：利用固定床微反应器对催化剂汞氧化性能进行研究，结合物化表征建立催化剂的构效关系，从而揭示氯化铜改性催化剂的抗硫机理。

结　论：1. $CuCl_2$ 的添加提升了催化剂的汞氧化性能：在 150-250 ^oC 温度区间内，催化剂的汞养护效率为 100%，含硫气氛下反应 320 分钟后锰铈氧化物的汞氧化效率由 100%下降到 78%，对于 $CuCl_2$ 改性催化剂来说，共氧化性能依旧维持在 100%；2. 对于锰铈氧化物催化剂来说，Mn^{4+}为主要的活性位点，对于 $CuCl_2$ 改性催化剂来说，除了 Mn^{4+} 外，Cl^-也是其中的活性位点；3. 含硫气氛下 Mn4+ 利用量的下降是导致锰铈氧化物催化剂活性下降的主要原因，而高反应活性 Cl^-的存在是导致 $CuCl_2$ 改性催化剂依旧保持高汞脱除效率的主要原因。

关键词：汞氧化；$CuCl_2$ 改性；锰铈氧化物纳米棒；抗硫性能；氧化活性